Polar nematic state in an iron-based superconductor $LaFeAsO_{1-x}H_x$

Sachiko Maki
Tokyo Institute of Technology
Jun-ichi Yamaura (jyamaura@lucid.msl.titech.ac.jp)
Tokyo Institute of Technology https://orcid.org/0000-0002-8992-9099
Soshi Iimura
Tokyo Institute of Technology
Hitoshi Abe
High Energy Accelerator Research Organization
Hajime Sagayama
High Energy Accelerator Research Organization
Reiji Kumai
High Energy Accelerator Research Organization https://orcid.org/0000-0002-5320-0028
Youichi Murakami
KEK
Satoru Matsuishi
Materials Research Center for Element Strategy
Hideo Hosono
Tokyo Institute of Technology https://orcid.org/0000-0001-9260-6728

Article

Keywords: Bipartite Magnetic Parent Phases, Phase Transitions, Superconductivity

Posted Date: September 29th, 2020

DOI: https://doi.org/10.21203/rs.3.rs-77544/v1

Abstract

High critical temperature (T_c) superconductivity is generally considered to result from a fluctuation-mediated Cooper-pairing derived from a parent phase. The question of what type of fluctuation forms in materials thus plays a key role in understanding the mechanism of superconductivity. The iron-based superconductor $LaFeAsO_{1-x}H_x$ possesses bipartite magnetic parent phases with centrosymmetric ($x \sim 0$) and non-centrosymmetric ($x \sim 0.5$) structures. The latter is an intriguing polar-metal phase induced by temperature and carrier doping. Here, we investigate average and local structures of $LaFeAsO_{1-x}H_x$ using X-ray diffraction and extended X-ray absorption fine-structure measurements. We found lattice C_4 symmetry breaking far above the structural transition temperature, and the signature of a tiny split in As–Fe bond distances with broken spatial inversion symmetry in a wide temperature/doping range. The former reveals a nematic state, and the latter highlights a fluctuated state of polar structure which can be appropriately called polar nematic state.

Introduction

Spatial inversion symmetry is intimately involved in the physics of matter, thereby its breaking can trigger exotic quantum phenomena. For example, metallic materials with polar crystallographic structure—polar metals—offer the opportunity to explore interesting physics such as unconventional superconductivity, nonreciprocal transport, and inverse Faraday effect[1–4]. While over 60 polar metals have been reported to date[5], a temperature-induced polar metal state as suggested by Anderson and Blount in 1965 is rare because screenings of conduction electrons hamper the formation of a macroscopic electrostatic field[6]. Shi *et al*. reported an example of a ferroelectric-like transition while maintaining the metallic behaviour in $LiOsO_3$[7]. On rising temperature or doping carrier, such a polar metal will recover its centrosymmetric structure; thus, one would expect a fluctuating state, a quantum critical point, and a nematic state adjacent to the polar metal phase[8–10].

Studies of high-T_c iron-based superconductors have experienced spectacular growth in condensed matter physics since their discovery[11–13]. We believe that the most promising material for studying polar metals is an iron oxypnictide $LaFeAsO_{1-x}H_x$, which is a hydrogen-substituted version of the prototype iron-based superconductor $LaFeAsO_{1-x}F_x$[14]. The $LaFeAsO_{1-x}H_x$ exhibits a characteristic phase diagram via electron doping, as illustrated in Fig. 1. The diagram has two magnetic parent phases at $x \sim 0$ (PP1) and $x \sim 0.5$ (PP2), and two superconducting domes with $T_{c,max}$ = 26 K at $x \sim 0.08$ (SC1) and $T_{c,max}$ = 36 K at $x \sim 0.35$ (SC2)[15–18]. Tetragonal-orthorhombic structural transitions at T_{s1} ($x \sim 0$) and T_{s2} ($x \sim 0.5$) precede magnetic transitions; the respective orthorhombic structures are centrosymmetric and non-centrosymmetric[18–20]. The PP2 structure with the polar point group *mm*2 serves as a unique parent phase in high-T_c materials as the spatial inversion symmetry is broken by temperature[18]. Throughout this paper, we use the term "parent phase" to refer to the magnetic ordered state that breaks lattice C_4 symmetry. The source of SC2 has been discussed in terms of spin-fluctuation, orbital-fluctuation, and

orbital-selective Mott state models[16,21–24]. However, the nematicity or fluctuating state in highly electron doped $LaFeAsO_{1-x}H_x$ remains unexplored and warrants investigation.

In this paper, we analyse the average and local structures of $LaFeAsO_{1-x}H_x$ ($0.35 \leq x \leq 0.51$) by measuring synchrotron X-ray diffraction (XRD) and extended X-ray absorption fine-structure (EXAFS). Our XRD and EXAFS results led us to identify a polar nematic state: a broken lattice C_4 symmetry and a polar fluctuated structure that emerge at temperatures far above the parent phase. These phenomena arise from the dynamical and short-range fluctuation of the parent phase structure.

Results And Discussion

We first focus on the change of crystal lattice symmetry in XRD measurements. Figure 2a shows the X-ray profiles for 220_T reflection at 300, 120, and 32 K for $x = 0.51$, where the suffix "T" signifies the indexing in the tetragonal system. Though the 220_T profile is supposed to split into two peaks below the tetragonal-orthorhombic structural transition at $T_{s2} \sim 95$ K, the profile was already broadened at 120 K. We regard the T_{s2} transition as static and long-range order of the orthorhombic distortion, the temperature of which was estimated using the lattice constant[18] and the resistivity[16] anomalies. Moreover, the profile with a shoulder at 32 K exhibits inequivalent intensities of two reflections split from 220_T, manifesting the presence of polar structure below T_{s2} (Supplementary Information, Fig. S1).

Figure 2b plots the temperature dependence of the profiles' full width at half maximum H for $x = 0.51$, 0.45, 0.42, 0.40, and 0.35. H was obtained by fitting a profile to a single pseudo-Voigt function and normalising it to room temperature values. The H values rise significantly when cooled past the T_{s2} transition for $x = 0.51$, 0.45, and 0.42. Note that they gradually increase far above T_{s2}. In contrast, the H values are nearly constant with temperature for $x = 0.40$ and 0.35. We here define the critical temperature T^* as the point deviating from the baseline formed from the averaged values of H above 250 K. The results are $T^* = 240$, 190, and 140 K for $x = 0.51$, 0.45, and 0.42, respectively. Since the T_{s2} transition entails the broadening of the 220_T peak, our result reveals a breaking of lattice C_4 symmetry for $x \geq 0.42$ despite a wide gap between T^* and T_{s2}. Considering the XRD measurement timescale of 10^{-15} s, the lowering of lattice symmetry in $T_s < T < T^*$ might be viewed as a slower dynamical phenomenon. Another possible symmetry lowering for $x = 0$ above $T_{s1} = 175$ K has been suggested in the narrow temperature range of 175 K < T < 200 K[25].

We proceed to examine the local structure of $LaFeAsO_{1-x}H_x$ from the As K-edge EXAFS measurement for $x = 0.51$, 0.45, 0.42, and 0.37. Figure 3a, b shows the representative k^2-weighted EXAFS oscillation $k^2\chi(k)$ and R-space magnitude of the Fourier transformation (FT), respectively, at 9.7 and 250 K for $x = 0.51$. In

the radial direction without phase-correction, the peak amplitudes around R = 2.1 and 2.9 Å correspond to As–Fe and As–La/As–O shells, respectively. We analysed the bond distances from the fit to the first As–Fe shell with an R-range of 1.85–2.30 Å based on the high-temperature $P4/mmm$ structure. Figure 3c plots the temperature dependence of the As–Fe distances, which decrease on cooling within the high-temperature range (> 100 K). However, for x = 0.51, 0.45, and 0.42 the upturns in bond distances on cooling were observed at respective temperatures of 95, 90, and 30 K, which correspond closely to T_{s2}. The elongation of bond distance below T_{s2} arises from the negative thermal expansion of the c-axis, as reported in previous XRD measurement[18].

Next, we employed a Fourier-filtered back transformation in EXAFS, which enables the detection of unknown tiny distortions within a specific coordination sphere[26,27]. Figure 4 illustrates the Fourier-filtered EXAFS amplitudes for As–Fe (1.60–2.45 Å) shells of R-spectra (EXAFS oscillations in Supplementary Information, Fig. S2). This examination found inflection points or “kinks” in each of profiles at the low temperature side. The amplitudes at the lowest temperature and at 250 K are plotted in the figure insets with solid blue and dashed black lines, respectively. The data at 250 K is normalised by the peak position and height of the object profiles used for the baseline. We define the difference amplitude between the object profiles and the baseline as the phenomenological formula $k^2\chi_{dif}(q) = k^2\chi(q)(T) - s_0 k^2\chi(s_1 q)(250\ \mathrm{K})$, where s_0 and s_1 are the scale factors (Supplementary Information, Fig. S3). We evaluated the kink positions q_{beat} indicated by arrows as the peaks in the wavenumber derivatives of $k^2\chi_{dif}(q)$. The q_{beat} values were roughly 11.2, 11.0, 11.6, and 11.3 $Å^{-1}$ respectively for x = 0.51, 0.45, 0.42, and 0.37 at the lowest temperature. The kink is due to the beat produced from the phase difference of EXAFS oscillations with the difference of bond distances ΔR in the shell. Based on the relation $\Delta R = \pi/(2q_{beat})$[26], we can estimate ΔR of the As–Fe distances to be 0.140, 0.143, 0.135, and 0.139 Å for x = 0.51, 0.45, 0.42, and 0.37, respectively.

The uniform As–Fe distance in the high-temperature phase splits into two long and two short distances in PP2 along with the loss of inversion symmetry[18], leading to a small ΔR; this was not observed in PP1[19,20]. Note that ΔR at 32 K for x = 0.51 in PP2 was previously determined to be 0.14 Å from XRD study[18], which agrees with our EXAFS result. We therefore ascribe the kinks in the EXAFS amplitude to the presence of local polar structure, and regard the $k^2\chi_{dif}(q)$ as the fraction of the polar structure. The amplitude is largest at 30 K for x = 0.51 in PP2; its value drops with decreasing x and/or rising temperature, but can still be observed far outside of PP2.

Our results from XRD and EXAFS are summarised in Fig. 1 together with the previously observed phase diagram[15,16,18]. The green area signifies the local distortion with broken inversion symmetry. The phase diagram shows that the lowering of lattice symmetry appears below T^*, and dynamical and short-range

polar structure emerges over wide ranges in temperature and doping. Taking account of the gradual changes in H and beat amplitude, their transformations may be regarded as cross-over phenomena instead of a phase transition.

In the iron-based superconductors $BaFe_2(As_{1-x}P_x)_2$ and $Sr_{1-x}Na_xFe_2As_2$, nematic states arise at specific doping levels from parent to superconducting phase, while breaking C_4 magnetic and/or lattice symmetries[28,29]. Hence, we view the lowering of lattice symmetry at temperatures $T_{s2} \leq T \leq T^*$ revealed by our XRD measurements as a nematic state. In the same way, we suggest that our nematic state involves an electronic or magnetic nematicity. Moreover, the local polar structure was identified over a wider temperature and doping range. Since the polar structure below T_{s2} entails the breaking of lattice C_4 symmetry, both of these phenomena that occur above T_{s2} should be intertwined. We thus propose that the $T_{s2} \leq T \leq T^*$ region can be called a polar nematic state, although it is difficult to identify the vanishing temperature for beat amplitude. Sakurai *et al*. reported NMR measurements for $LaFeAsO_{1-x}H_x$ and pointed out an anisotropy of the electric-field gradient derived from a disproportionation of *d*-orbital electrons[30]. This observation likely shares a close link with our result, given the possibility of the local polar structure being related to an orbital ordering or its fluctuation. Moreover, Onari *et al*. theoretically proposed that the second parent phase comes from a charge quadrupole order stemming from the disproportionation of *d*-orbital electrons[23].

Let us now consider the interplay between the local polar structure and the superconductivity. Lowering of lattice symmetry was unobserved via XRD for x = 0.40 and 0.35 in SC2, whereas the local polar structure was detected via EXAFS for x = 0.37. Since the orthorhombicity in PP2 rapidly reduces with decreasing x from x = 0.51[18], the presence of a minute lattice distortion may have been experimentally undetectable via XRD. Regardless, the aforementioned electric-field gradient anisotropy from NMR[30] was evident even in the superconducting phase. Hence, we suggest that the polar nematic state is linked with the superconducting phase[30]. We consider SC2 to be derived from PP2 by the introduction of holes, namely as x decreases from ~ 0.5. Thus, in relation to superconductivity, the polar structure may have an effect on T_c or the paring mechanism. As an example, noncentrosymmetric superconductors can give rise to exotic pairing states with spin-singlet and spin-triplet mixtures[1,31]. In contrast, the superconductivity in $LaFeAsO_{1-x}H_x$ emerges after recovering inversion symmetry, where one might expect fluctuation-related phenomena instead. Intriguing theories have been proposed by Anderson and Blount[6], and Ydlium *et al*.[32] positing that ferroelectric-like soft phonons enhance T_c or drives the superconductivity. Moreover, an odd-parity superconductivity derived from parity fluctuation has been predicted in the vicinity of inversion symmetry breaking[33,34]. Since polar structure is also observed in $SmFeAsO_{1-x}H_x$ with T_c = 55 K[35,36], further insight awaits from the more detailed investigation of local physical properties in this system.

In conclusion, the average and local structures for highly electron doped $LaFeAsO_{1-x}H_x$ with bipartite parent phases were investigated using XRD and EXAFS measurements. The second parent phase (x ~ 0.5) entails the time-reversal and the spatial inversion symmetries broken. We have demonstrated that a

dynamical state with broken lattice C_4 symmetry and polar structure—a polar nematic state—emerges in a wide temperature/doping range above the parent and the superconducting phases. This observation reported in this study is the intriguing result because the electronic, magnetic, and lattice instabilities should be weak generally in the highly electron-doped region. We conclude that EXAFS serves as a good probe for the detection of local polar structure that could help map further studies of nematicity.

Methods

Powder samples of $LaFeAsO_{1-x}H_x$ were prepared using a high-pressure solid-state reaction as described in a previous study[15]. Synchrotron XRD and As K-edge transmission EXAFS were carried out over the whole temperature range on beamlines BL-8A/8B/9C at the Photon Factory at the High Energy Accelerator Research Organization (KEK). For XRD measurements, a very fine powder sample was enclosed in a capillary with a diameter of 0.1 mm, which was irradiated with an X-ray beam. The sample was continuously rotated during the exposure. Two-dimensional XRD images were obtained using a diffractometer with a curved imaging plate (R-AXIS, Rigaku Corp.) at wavelength λ = 1.0993 Å. The images were integrated to yield 2θ-intensity data using the DISPLAY software (Rigaku). For EXAFS measurements, all crystalline reagents were fastidiously mixed with BN powder. This process is key to obtaining high-quality data up to the high-k region. EXAFS oscillations and R-space magnitude of the Fourier transformation were extracted from the raw data using the Athena program. The R-space data were fitted to the theoretical signals calculated by FEFF8 code using IFEFIT on the Arthemis platform[37].

Declarations

Author Contributions

S.Maki, J.Y, S.I., Y.M, S. Matsuishi, H.H conceived the study. S.I. synthesised the samples. S.Maki, J.Y., H.A, H.S, R.K performed the synchrotron X-ray measurements. S.Maki, J.Y co-wrote the manuscript. All the authors discussed the results and the manuscript.

Acknowledgements

We thank Y. Kuramoto for fruitful discussions. This work was supported by the MEXT Elements Strategy Initiative to Form Core Research Center (JPMXP0112101001) and JSPS KAKENHI (No. 16K05434). The synchrotron XRD, EXAFS and neutron scattering experiments were performed with the approval of the Photon Factory Program Advisory Committee (No. 2013S2-002 and 2016S2-004) of IMSS, KEK. The crystal structures were created using the software VESTA [38].

References

1. *Non-Centrosymmetric Superconductors-Introduction and Overview*, edited by Bauer, E. & Sigrist, M. (Springer, Heidelberg, 2012).
2. Kim, T. H. et al. Polar metals by geometric design. *Nature* **533**, 68–72 (2016).
3. Ideue, T. et al. Bulk rectification effect in a polar semiconductor. *Nat. Phys.* **13**, 578–583 (2017).
4. Edelstein, V. M. Inverse Faraday Effect in Conducting Crystals Caused by a Broken Mirror Symmetry. *Phys. Rev. Lett.* **80**, 5766–5769 (1998).
5. Benedek, N. A., Birol, T. 'Ferroelectric' metals reexamined: fundamental mechanisms and design considerations for new materials. *J. Mater. Chem. C* **4**, 4000–4015 (2016),
6. Anderson, P. W., Blount, E. I. Symmetry Considerations on Martensitic Trans Formations: "Ferroelectric" Metals ? *Phys. Rev. Lett.* **14**, 217 (1965).
7. Shi, Y. et al. A ferroelectric-like structural transition in a metal, *Nat. Mat.* **12**, 1024–1027, (2013).
8. Volkov, P. A., Chandra, P. Multiband Quantum Criticality of Polar Metals. *Phys. Rev. Lett.* **124**, 237601 (2020).
9. Rischau, C. W., Lin, X., Grams, C. P., Finck, D., Harms, S. A ferroelectric quantum phase transition inside the superconducting dome of $Sr_{1-x}Ca_xTiO_{3-\delta}$. *Nat. Phys.* **13**, 643–648 (2017).
10. Kobayashi, T. C., Irie, Y., Yamaura, J., Hiroi, Z., Murata, K. Superconductivity of Heavy Carriers in the Pressure-Induced Phases of $Cd_2Re_2O_7$. *J. Phys. Soc. Jpn.* **80**, 023715 (2011).
11. Lee, A. P., Nagaosa, N., Wen, X.-G. Doping a Mott insulator: Physics of high-temperature superconductivity. *Rev. Mod. Phys.* **78**, 17–85 (2006).
12. Paglione, J., Greene, R. L. High-temperature superconductivity in iron-based materials. *Nat. Phys.* **6**, 645–658 (2010).
13. Hosono, H., Kuroki, K. Iron-based superconductors: Current status of materials and pairing mechanism. Physica *C* **514**, 399–422 (2015).
14. Kamihara, Y., Watanabe, T., Hirano, M., Hosono, H. Iron-based layered superconductor $La[O_{1-x}F_x]FeAs$ (x = 0.05–0.12) with T_c = 26 K. *J. Am. Chem. Soc.* **130**, 3296–3297 (2008).
15. Iimura, S. et al. Two-dome structure in electron-doped iron arsenide superconductors. *Nat. Commun.* **3**, 943 (2012).
16. Iimura, S. et al. Heavy electron doping induced antiferromagnetic phase as the parent for the iron oxypnictide superconductor $LaFeAsO_{1-x}H_x$. *Phys. Rev. B* **94**, 024512 (2016).
17. Fujiwara, N. et al. Detection of antiferromagnetic ordering in heavily doped $LaFeAsO_{1-x}H_x$ pnictide superconductors using nuclear-magnetic-resonance techniques. *Phys. Rev. Lett.* **111**, 097002 (2013).
18. Hiraishi, M. et al. Bipartite magnetic parent phases in the iron oxypnictide superconductor. *Nat. Phys.* **10**, 300–303 (2014).
19. de la Cruz, C. et al. Magnetic order close to superconductivity in the iron-based layered $LaO_{1-x}F_xFeAs$ systems. *Nature* **453**, 899–902 (2008).

20. Qureshi, N. et al. Crystal and magnetic structure of the oxypnictide superconductor $LaFeAsO_{1-x}F_x$: A neutron-diffraction study. *Phys. Rev. B* **82**, 184521 (2010).
21. Suzuki, K. et al. Model of the Electronic Structure of Electron-Doped Iron-Based Superconductors: Evidence for Enhanced Spin Fluctuations by Diagonal Electron Hopping. *Phys. Rev. Lett.* **113**, 027002 (2014).
22. Moon, C.-Y., Park, H., Haule, K., Shim, J. H. Origin of doping-induced suppression and reemergence of magnetism in $LaFeAsO_{1-x}H_x$. *Phys. Rev. B* **94**, 224511 (2016).
23. Onari, S., Yamakawa, Y. Kontani, H. High-T_c Superconductivity near the Anion Height Instability in Fe-Based Superconductors: Analysis of $LaFeAsO_{1-x}H_x$. *Phys. Rev. Lett.* **112**, 187001 (2014).
24. Kobayashi, K. et al. Pressure effect on iron-based superconductor $LaFeAsO_{1-x}H_x$: Peculiar response of 1111-type structure. *Sci. Rep.* **6**, 39646 (2016).
25. McGuire, M. A. et al. Phase transitions in LaFeAsO: Structural, magnetic, elastic, and transport properties, heat capacity and Mössbauer spectra. *Phys. Rev. B* **78**, 094517 (2008).
26. Zhang, C. J., Oyanagi, H. Local lattice instability and superconductivity in $La_{1.85}Sr_{0.15}Cu_{1-x}M_xO_4$ (M = Mn, Ni, and Co). *Phys. Rev. B* **79**, 064521 (2009).
27. Niemann, W. Multishell Beat-Node Method for EXAFS. *Physica B* **158**, 279–281 (1989).
28. Kasahara, S. et al. Electronic nematicity above the structural and superconducting transition in $BaFe_2(As_{1-x}P_x)_2$. *Nature* **486**, 382–385 (2012).
29. Frandsen, B. A. et al. Widespread orthorhombic fluctuations in the $(Sr,Na)Fe_2As_2$ family of superconductors. *Phys. Rev. B* **98**, 180505(R) (2018).
30. Sakurai, R. et al. Quantum critical behavior in heavily doped $LaFeAsO_{1-x}H_x$ pnictide superconductors analyzed using nuclear magnetic resonance. *Phys. Rev. B* **91**, 064509 (2015).
31. Bauer, E. et al. Heavy Fermion Superconductivity and Magnetic Order in Noncentrosymmetric $CePt_3Si$. *Phys. Rev. Lett.* **92**, 027003 (2004).
32. Yildirim, T. Ferroelectric soft phonons, charge density wave instability, and strong electron-phonon coupling in BiS_2 layered superconductors: A first-principles study. *Phys. Rev. B* **87**, 020506(R) (2013)
33. Kozii, V., Fu, L. Odd-Parity Superconductivity in the Vicinity of Inversion Symmetry Breaking in Spin-Orbit-Coupled Systems. *Phys. Rev. Lett.* **115**, 207002 (2015).
34. Wang, Y., Cho, G. Y., Hughes, T. L., Fradkin, E. Topological superconducting phases from inversion symmetry breaking order in spin-orbit-coupled systems. *Phys. Rev. B* **93**, 134512 (2016).
35. Matsuishi, S. et al. Controlling factors of T_c dome structure in 1111-type iron arsenide superconductors. *Phys. Rev. B* **89**, 094510 (2014).
36. Iimura, S. et al. Large-moment antiferromagnetic order in overdoped high-*T*c superconductor $^{154}SmFeAsO_{1-x}D_x$. *Proc. Natl. Acad. Sci. USA* **114**, E4354–E4359 (2017).
37. Ravel, B., Newville, M. ATHENA, ARTEMIS, HEPHAESTUS: data analysis for X-ray absorption spectroscopy using IFEFFIT. *J. Synchrotron Rad.* **12**, 537–541 (2005).

38. Momma, K., Izumi, F. VESTA†3 for three-dimensional visualization of crystal, volumetric and morphology data. *J. Appl. Crystallogr.* **44**, 1272–1276 (2011).

Figures

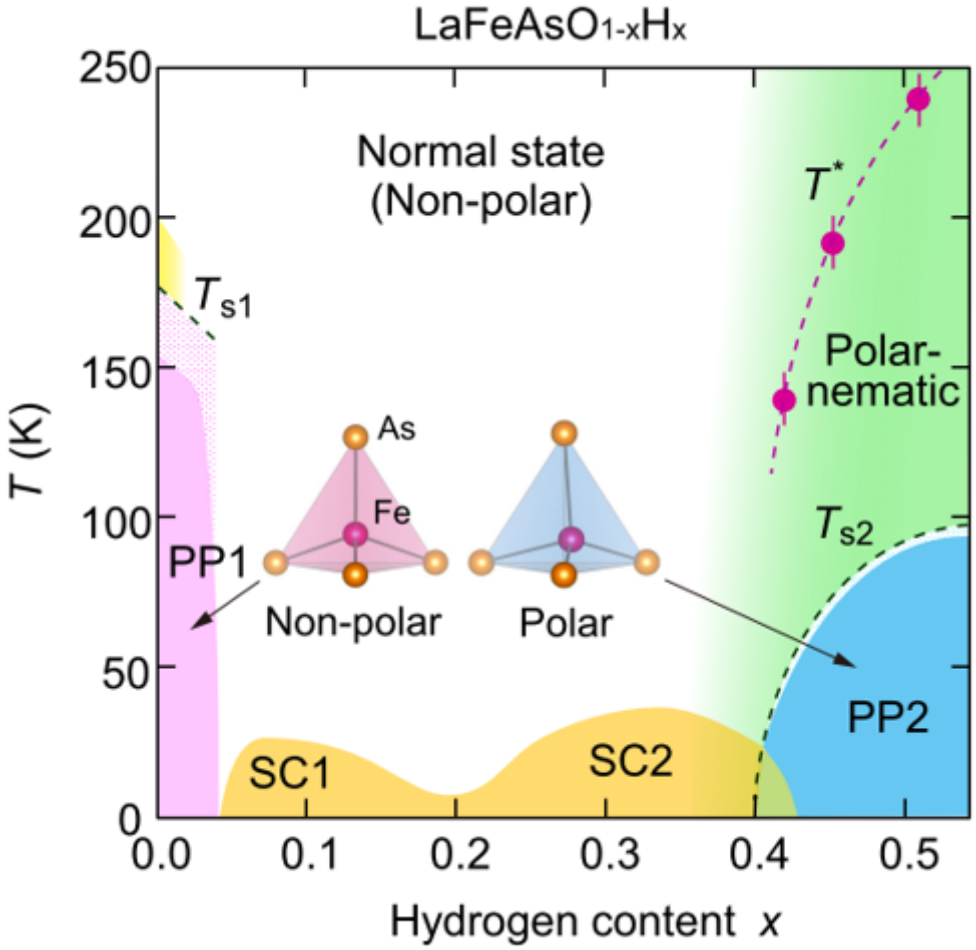

Figure 1

Magnetic, structural, superconducting phase diagram and polar nematic state for LaFeAsO1−xHx. The regions marked PP1 and PP2 signify the first (x ~ 0) and second (x ~ 0.5) antiferromagnetic parent phases with centrosymmetric and noncentrosymmetric structures, respectively. The tetragonal-orthorhombic structural transitions at Ts1 and Ts2 (black dashed lines) emerge just above the antiferromagnetic transitions. The SC1 and SC2 represent the first and second superconducting phases with maximum critical temperatures at Tc = 26 K (x = 0.08) and 36 K (x = 0.35), respectively. While the crystal in PP1 holds inversion symmetry (space group: Cmme) with a uniform Fe−As distance, the inversion symmetry is broken in PP2 (space group: Aem2), leading to two long and two short Fe−As distances. XRD reveals the nematic state with broken lattice C4 symmetry below T* (magenta circles). The error of T* is taken as the width of its adjacent points. EXAFS measurement unveils local distortion with broken inversion symmetry (green area). The temperature/doping range Ts2 < T < T* is regarded as

the polar nematic state. Possible lowering of lattice symmetry above Ts1 was also observed for x = 0 (yellow area).

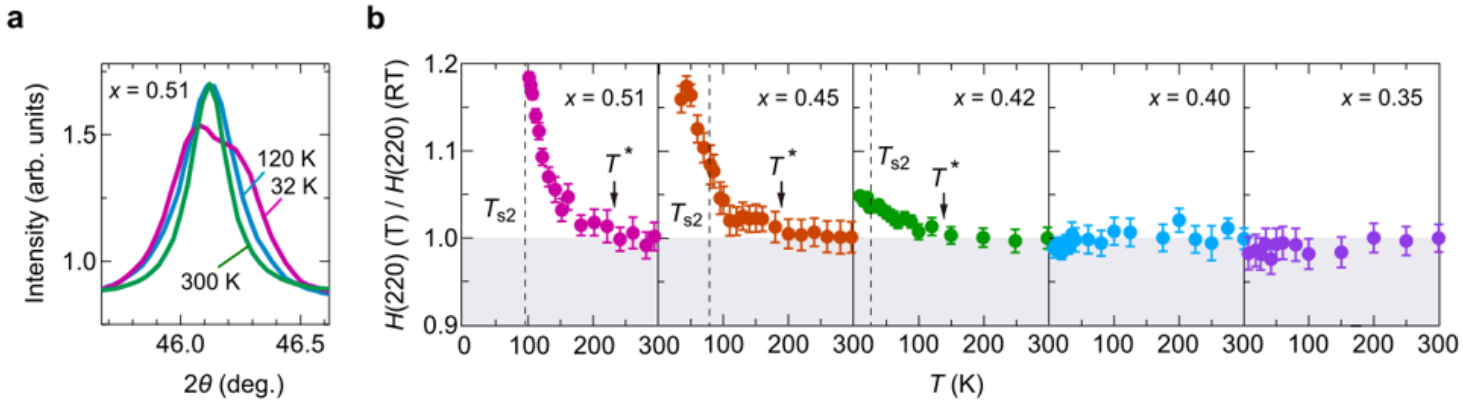

Figure 2

X-ray profiles and FWHM of 220T reflections. a X-ray profile for 220T reflection for LaFeAsO1−xHx (x = 0.51) which splits into two peaks in the orthorhombic phase. b Temperature dependence of full width at half maximum H(220) normalised by the data at room temperature for 220T reflections in x = 0.51, 0.45, 0.42, 0.40, and 0.35. Ts2 is deemed as the static tetragonal-orthorhombic structural transitions. T* represents the point of broken lattice C4 symmetry. The error bars in b signify the uncertainly in the least-squares fitting of the profiles.

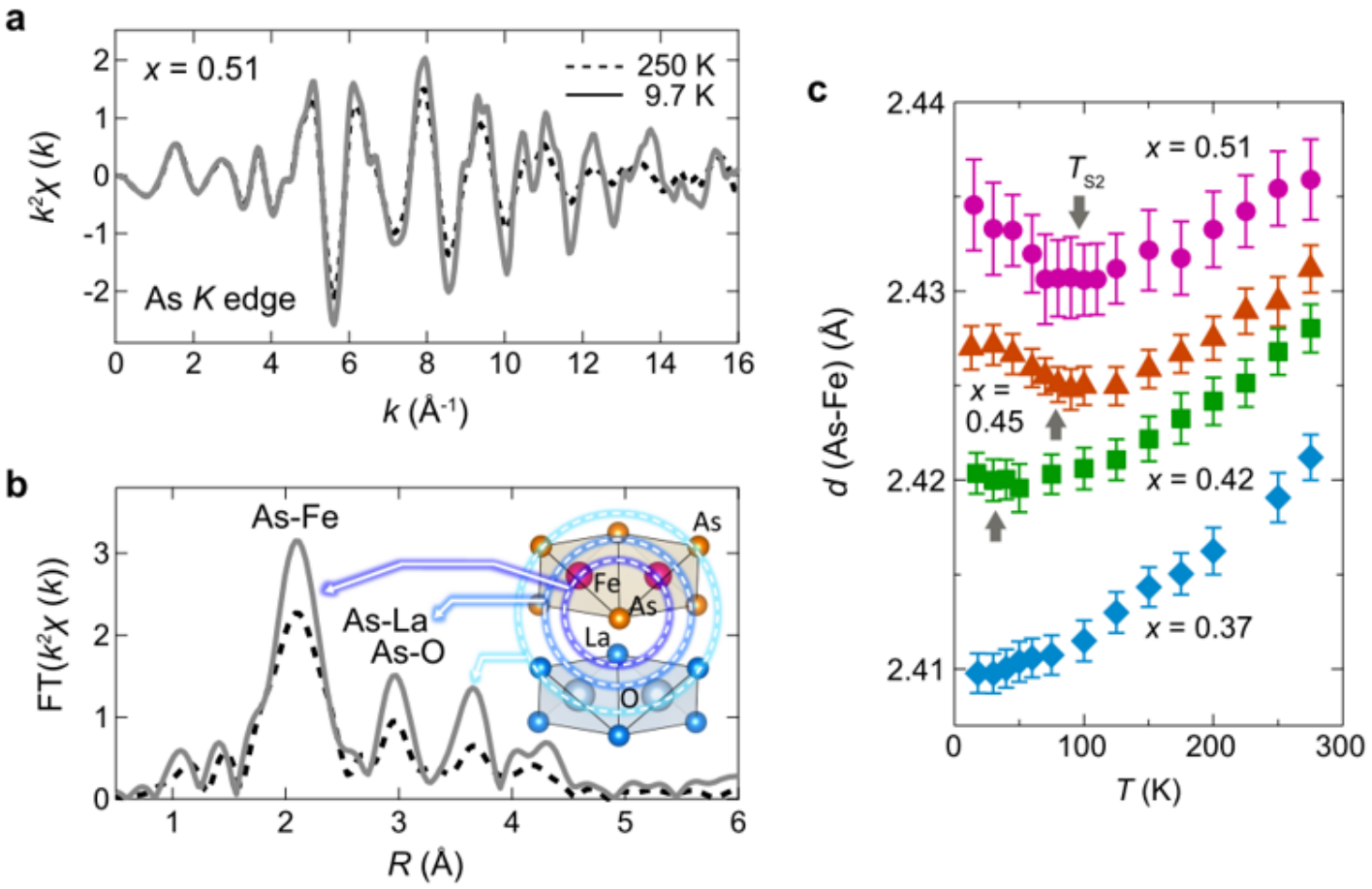

Figure 3

EXAFS oscillations, R-space amplitudes, and As-Fe distances. a k2-weighted EXAFS oscillation k2χ(k) of LaFeAsO1−xHx at 250 K (dotted line) and 9.7 K (solid line) for x = 0.51 at the As K-edge. b Magnitudes of Fourier transformed R-spectra from oscillation profiles without phase corrections. Inset represents the corresponding shells from the central As atoms. c Temperature dependence of As−Fe distance for x = 0.51, 0.45, 0.42, and 0.37, estimated from fitting R-spectra for the Fe shell in the range 1.85–2.30 (Å). The Ts2 transitions were taken from the literature16,18. The error bars in c represent the uncertainly in the least-squares fitting of the R-spectra.

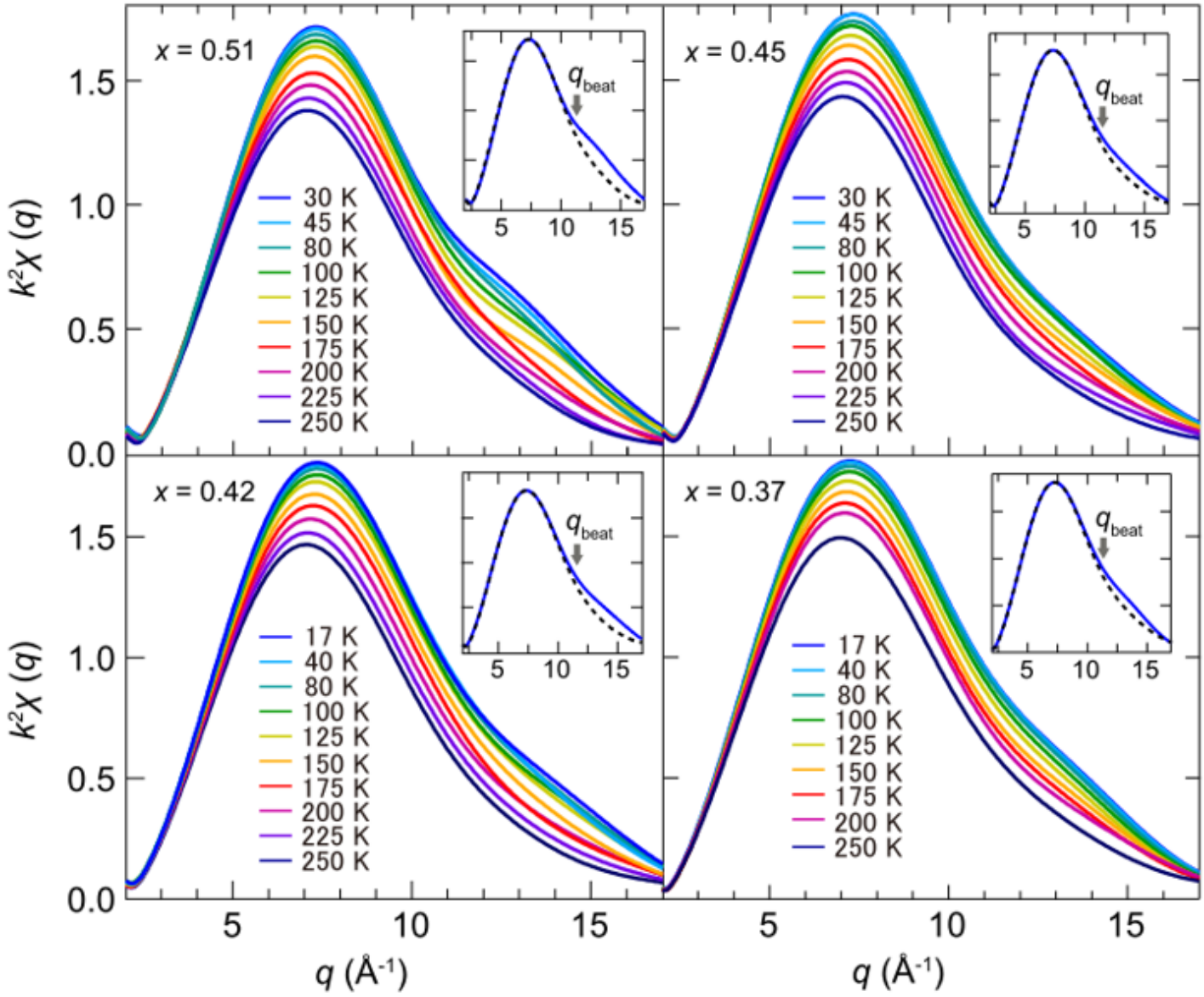

Figure 4

Fourier-filtered EXAFS amplitudes. Fourier-filtered EXAFS amplitudes transformed in the window of 1.60–2.45 Å for As−Fe shell R-spectra. Inset shows the amplitudes at the lowest temperature (blue solid line) and 250 K (black dashed line). The latter profile is shifted to coincide with the maximum of the lowest

temperature data. Kinks at the lowest temperatures, labelled qbeat and indicated by arrows, are observed at qbeat ~ 11.2, 11.0, 11.6, and 11.3 Å-1 for x = 0.51, 0.45, 0.42, and 0.37, respectively.

Supplementary Files

This is a list of supplementary files associated with this preprint. Click to download.

- La1111PolarNematicSupplementary.docx